Extension of HAMS with the generalized modes approach

Raghavan, V.; Metrikine, A. V.; Lavidas, G.; Islam, T.; Venugopal, V.

Citation (APA)
Raghavan, V., Metrikine, A. V., Lavidas, G., Islam, T., & Venugopal, V. (2024). Extension of HAMS with the generalized modes approach. In C. G. Soares, & S. Wang (Eds.), *Innovations in Renewable Energies Offshore - Proceedings of the 6th International Conference on Renewable Energies Offshore, RENEW 2024* (pp. 193-199). CRC Press / Balkema - Taylor & Francis Group. https://doi.org/10.1201/9781003558859-22

Important note
To cite this publication, please use the final published version (if applicable).
Please check the document version above.

Extension of HAMS with the Generalized Modes approach

V. Raghavan, A.V. Metrikine & G. Lavidas
Department of Hydraulic Structures
Delft University of Technology, Netherlands

T. Islam & V. Venugopal
Institute for Energy Systems (IES), School of Engineering
The University of Edinburgh, UK

ABSTRACT: The Boundary Element Method (BEM) based on the linear potential flow theory has shown to produce accurate results at low computational costs in numerical modelling of the hydrodynamics of Wave Energy Converters (WECs). WAMIT , Nemoh and Capytaine are some of the most popular frequency domain BEM solvers used in the response analysis of various WECs. Hydrodynamic Analysis of Marine Structures (HAMS), another open-source BEM solver gaining traction, has been applied to the analysis of single WECs considering rigid body motions providing highly accurate solutions at lower computational costs as compared to other solvers. This research extends its current capabilities to model structures with constraints by applying the generalized modes approach Results presented include of a cross-model validation with commercial solver WAMIT, of the hydrodynamic coefficients and exciting forces considering flap converter. Furthermore, a comparison is shown with popular open-source solver Capytaine for the same case, since it has parallelization.

1 INTRODUCTION

The strategy from the European Union has targets to deploy 40 GW of wave energy by 2050 (EC 2020). In order the achieve these set targets, research into lowering the Levelized Cost of Energy (LCOE) for WECs is essential. One of the key aspects here is to advance the numerical techniques that can simulate the behavior of all types of WECs at low computational costs.

Over the last two decades, many WEC designs have been proposed with a wide range of energy conversion principles (e.g. oscillating water column, attenuator, oscillating surge converter, overtopping) (Falcão 2010). Historically, most WECs were designed assuming rigid body motions, however recent WEC research efforts have brought attention to the design of flexible structures as a way of lowering the cost of energy (van Rij et al. 2017). Furthermore, when modelling WECs such as the oscillating surge converter/flap, the consideration of the hinge constraint at the bottom is important to assess the hydrodynamics of the structure (Gomes et al. 2015). Therefore, numerical techniques that can model the fluid structure interaction with a flexible structure/structure with constraint is important.

BEM based on linear potential flow theory is one of the most popular numerical methods for simulating the hydrodynamics of structures within the field of wave energy, since it has good accuracy at low computational costs. There are many well established commercial codes such as WAMIT (Lee & Newman 2006) and ANSYS AQWA (ANSYS 2012), as well as open-source codes such as Nemoh (Babarit & Delhommeau 2015) and Capytaine (Ancellin & Dias 2019).

When modelling flexible WECs or WECs with constraints, the 'Generalized modes approach' proposed by Newman (1994) is one of the most powerful techniques implemented within the BEM framework. This has been extensively used with the commercial solver WAMIT. Gomes et al. (2015) used this approach in WAMIT to study a bottom hinged flap subjected to regular and irregular waves for assessing power extraction and capture width ratio. The modelling approach utilized a combination of the generalized modes approach with a thin plate modelled with dipole panels in BEM. Sismani & Loukogeorgaki (2020) modelled and evaluated the response and power of a wave energy conversion system with multiple flaps in WAMIT, wherein additional mode shapes based on the displacement of each individual flap were captured within the hydrodynamics of the system. This has also been implemented in open-source BEM solvers. The generalized modes ap-

proach was used to investigate the design of a bottom fixed pressure-differential wave energy converter using Nemoh (Babarit et al. 2017). More recently, the S3 wave energy converter (a bulging horizontal cylinder) was modelled with Capytaine considering up to 4 modes (Ancellin et al. 2020).

HAMS (Liu 2019) is a recently developed open-source solver, that is still being established in the field. It has shown to be highly accurate and computationally efficient when compared with established solvers such as WAMIT and Nemoh. The work of Raghavan et al. (2022) compared HAMS, WAMIT and Nemoh (v2.x) considering the diffraction and radiation problem for two cases - a cylindrical point absorber and a flap WEC. It was observed that HAMS was overall closer to WAMIT as compared to Nemoh for both the cases. Furthermore, when comparing the computational effort, it was observed that HAMS was up to 21 times faster than Nemoh and 1-2 times faster than WAMIT (even when parallelization was considered). The work of Sheng et al. (2022) showed that HAMS provides better accuracy than Nemoh, as well as better speed of simulations as compared to both WAMIT and Nemoh when no parallelization is implemented. They tested several cases of a semi-immersed cylindrical point buoy, the TALOS WEC, a semi-immersed cylindrical point buoy with a heave plate, semi-immersed cylindrical point buoy, with gaps and semi-immersed cylindrical point buoy with overlapping panels. Furthermore, when creating models with thin structures (such as a heave plate) and overlapping panels (examples include joints of structures, modelling an OWC in a two-body system where the internal water column modelled as a piston overlaps with the hull of the OWC), HAMS matched the accuracy of WAMIT, while Nemoh is unable to deal diffraction-radiation computation when panels there are overlapping panels.

HAMS is currently only capable of analysing single floating structures for 6 rigid body modes. This research extends its current capabilities to model structures with constraints by applying the generalized modes approach thus making it capable of analyzing WECs such as the attenuators or a flap within a computationally efficient open-source framework. Cross-model validation is performed with the commercial solver WAMIT for the hydrodynamic coefficients and exciting forces. Furthermore, a comparison is also made with open-source solver Capytaine since both these solvers can utilize parallelization.

2 CURRENT NUMERICAL FRAMEWORK IN HAMS

HAMS is a BEM solver based on the three dimensional linear potential flow theory that assumes the flow to be inviscid, irrotational, incompressible and free of separation effects (Liu 2019, Liu et al. 2018). As mentioned earlier, HAMS is currently capable of

only analysing wave structure interaction with floating structure. The flow is described through a complex spatial velocity potential $\varphi(X)$ where $X = (X, Y, Z)$ are the global cartesian coordinates. The potential is decomposed into three parts: the incident wave potential $\varphi_i(X)$, the diffracted wave potential $\varphi_D(X)$, and the radiated wave potential $\varphi_j(X)$.

The considered domain has boundary conditions on the free surface (where the waves interact with the floating structure), the rigid sea bottom, the surface of the structure and the far field (Sommerfield's radiation condition). The potentials φ_l ($l = D$ or $l = j$) satisfy the Laplace equation (Liu 2019) in the entire fluid domain and are subjected to these boundary conditions on the free surface (Eqn 1), the sea bottom (Eqn 2), and on the body (Eqn 3 and Eqn 4) and the far field (Eqn 5):

$$\frac{\partial \varphi_l}{\partial z} - K\varphi_l = 0 \tag{1}$$

$$\frac{\partial \varphi_l}{\partial z} = 0 \tag{2}$$

$$\frac{\partial \varphi_D}{\partial n} = 0 \tag{3}$$

$$\frac{\partial \varphi_j}{\partial n} = n_j \tag{4}$$

$$\lim_{R \to \infty} \sqrt{KR}\left(\frac{\partial \varphi_l}{\partial R} - iKR\right) = 0 \tag{5}$$

where $K = \omega^2/g$ is the deep water wave number, g is the acceleration due to gravity.

Eqn 4 is applicable for the 6 rigid body modes, where n_j is the projection of the normal vector in each of the 6 degrees of freedom . Green's theorem is utilized to form the boundary integral equations for the diffraction and radiation potentials on the body boundary. The corresponding boundary value problem is, then, solved based on a 3D low-order panel method.

3 IMPLEMENTATION OF GENERALIZED MODES

In this section, the implementation of the generalized modes is explained based on the work of Newman (1994).

Table 1: Properties of the flap(all dimensions in m)

Part	Dimension ($W \times T \times H$)
Flap top	
Rectangular box	$18 \times 1.8 \times 8.5$
Triangular box	$18 \times 0 - 1.8 \times 0.9$
Flap bottom	
Rectangular box	$18 \times 1.8 \times 1.5$

3.1 Body boundary condition for the first order boundary value problem

The body boundary condition (Eqn 4) can also be expressed as a general expression:

$$\frac{\partial \varphi_j}{\partial n} = \mathbf{S_j}.\mathbf{n} \tag{6}$$

where S_j is a 3D vector shape function with cartesian components u_j, v_j, w_j and $\mathbf{n} = (n_x, n_y, n_z)$ is the normal vector projecting from the body towards the fluid Newman (1994). For the rigid body translational degrees of freedom ($j = 1,2,3$), the shape function is unit vector in the corresponding direction, and for the rigid body rotations (j=4,5,6), $\mathbf{S_j} = \mathbf{S_{j-3}} \times \mathbf{r}$, where $\mathbf{r}$ is the lever arm vector with respect to a rotation center(Newman 1994, Sismani and Loukogeorgaki 2020).

The projection of the normal vector can be written in general as:

$$\mathbf{S_j}.\mathbf{n} = u_j n_x + v_j n_j + w_j n_z \tag{7}$$

Therefore, by deriving this vector shape function for any additional mode/degree of freedom, the radiation and diffraction problem can also be solved considering this degree of freedom in HAMS. The vector shape function can represent general mode shapes corresponding to structural deflections, the motions of the interior free surfaces inside moonpools, or multiple bodies with constraints (Lee & Newman 2003).

3.2 Derivation of the shape function for a flap

The rigid flap from the work of Van 'T Hoff (Van 'T Hoff 2009) is used as a case study here for verification. The geometry is shown in Figure 2. The flap top combines two geometries, a rectangular box and a triangular box, while the flap bottom, which is rigidly fixed to the sea bottom, is composed of a rectangular box. The dimensions of these parts is shown in Table 1. The hinge is located at $L_s = 8.9$ m from the free surface. The water depth is 10.9 m, thus the hinge being at 2 m above the sea bottom.

XYZ is the global coordinate system. xyz is the local coordinate system located at the top of the flap and coincides with the global coordinate system, $x_d y_d z_d$ is the deformed coordinate system due to the flap's unit rotation θ. The flap is aligned such that the width (W) is along the Y axis. The surface of the flap is discretized into panels.

The global position vector $\mathbf{U_f} = (U_{f,x}, U_{f,y}, U_{f,z})$ of a random panel can be obtained based on the work of Sismani & Loukogeorgaki (2020) and is given as:

$$U_{f,x} = L_s sin\theta + X cos\theta - Z sin\theta \tag{8a}$$

$$U_{f,y} = Y \tag{8b}$$

$$U_{f,z} = -L_s(1 - cos\theta) + X sin\theta + Z cos\theta) \tag{8c}$$

Here X, Y, Z can be directly utilized as it aligns with x, y, z. The position vector of the hinge $\mathbf{U_h}$ is given as:

$$\mathbf{U_h} = (0, 0, -L_s) \tag{9}$$

Since we want to use the pitch rotation of the rigid flap top about the hinge, the lever arm vector $\mathbf{r}$ needs to be derived which is given as:

$$\mathbf{r} = \mathbf{U_f} - \mathbf{U_h} \tag{10}$$

with $\mathbf{r} = (r_x, r_y, r_z)$ where

$$r_x = L_s sin\theta + X cos\theta - Z sin\theta \tag{11a}$$

$$r_y = Y \tag{11b}$$

$$r_z = L_s cos\theta + X sin\theta + Z cos\theta \tag{11c}$$

The normal vector for the considered panel in the deformed state is given as:

$$\mathbf{n_f} = (n_{i,x} cos\theta - n_{i,z} sin\theta, n_{i,y},$$

$$n_{i,x} sin\theta + n_{i,z} cos\theta) \tag{12}$$

where $\mathbf{n_i} = (n_{i,x}, n_{i,y}, n_{i,z})$ is the normal vector of the considered panel in the undeformed state. The normal vector for the rigid body rotation for the pitch about the hinge can then be obtained as the y component of the cross product $\mathbf{r} \times \mathbf{n_f}$ (since the pitching occurs about the y-axis), which is obtained as:

$$n_{7,top} = n_{i,x}(L_s + X sin2\theta + Z cos2\theta)$$

$$+ n_{i,z}(-X cos2\theta + Z sin2\theta) \tag{13}$$

which for unit rotation (small angle approximation) can be reduced to

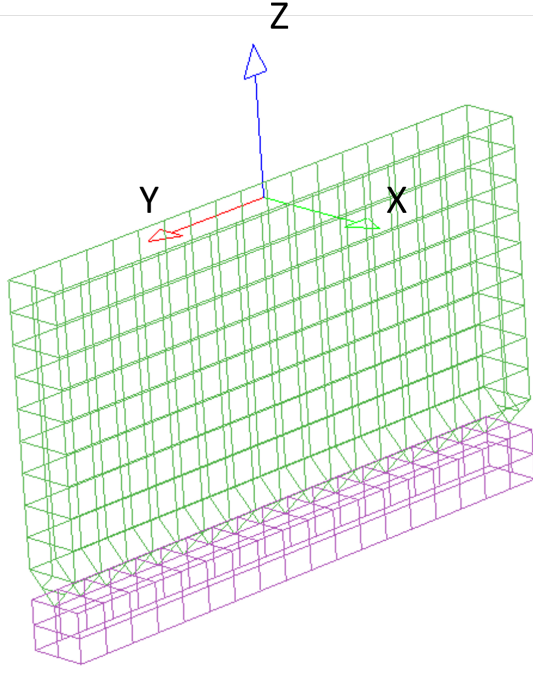$$n_{7,top} = n_{i,x}(L_s + Z) + n_{i,z}(-X) \tag{14}$$

Figure 1: Mesh of the flap in HAMS with 518 panels - Top (green) and bottom (pink)

From this the shape function for the additional degree of freedom/mode shape for the flap top can be obtained as:

$$\mathbf{S_{7,top}} = (L_s + Z, 0, -X) \qquad (15)$$

Since the flap bottom is stationary, the shape function for the bottom is a null vector.

$$\mathbf{S_{7,bottom}} = (0, 0, 0) \qquad (16)$$

Using this as the body boundary condition for the additional pitch motion about the hinge, the radiation and diffraction problems can be solved to obtain the hydrodynamic coefficients and excitation forces.

4 VALIDATION AND DISCUSSION

The cross-model validation with the commercial solver WAMIT was performed. Furthermore, a comparison with open-source solver Capytaine was also performed here.

As mentioned earlier, the considered geometry and results for the hydrodynamic coefficients and excitation force for the flap, were taken from the work of Van 'T Hoff (Van 'T Hoff 2009). The same resolution mesh (518 panels considering flap top and bottom) is utilized in both HAMS and Capytaine, based on the WAMIT model. In WAMIT, the flap was modelled as a two body problem, wherein the flap top (see Figure 2) is given a single degree of freedom of pitch with the center of rotation at the hinge ($z = -8.9$ m). The flap bottom is modelled as a stationary body with no degrees of freedom for the radiation problem,
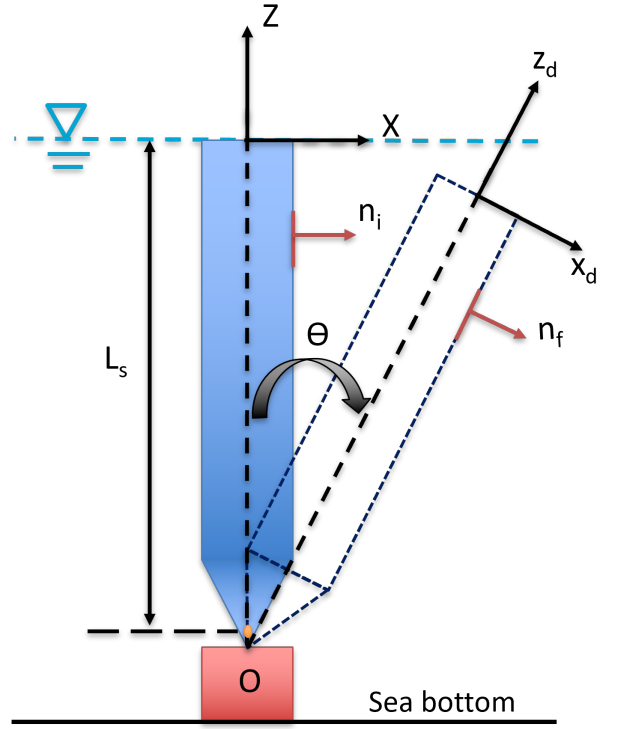

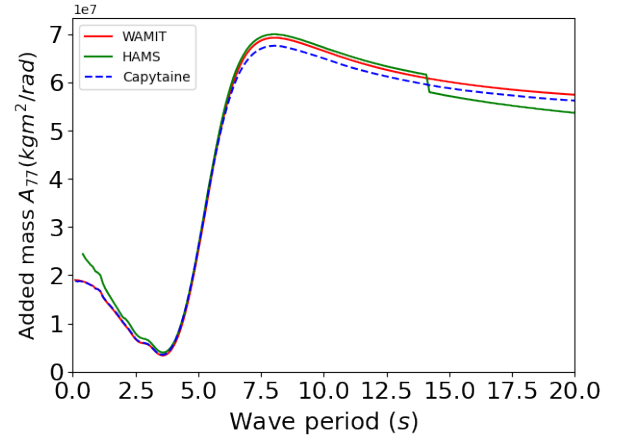Figure 2: Schematic representation of rotation of the flap

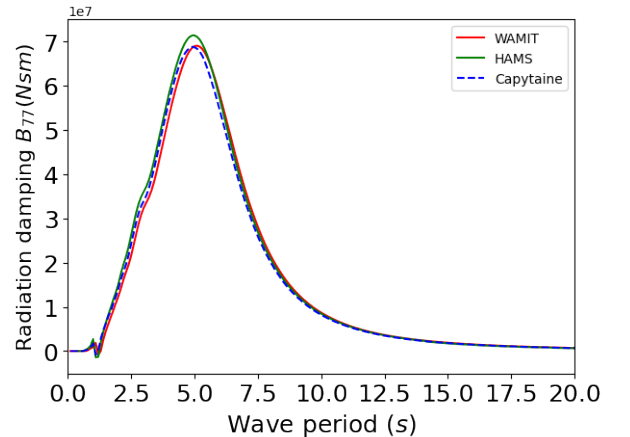Figure 3: Added mass flap A_{77}

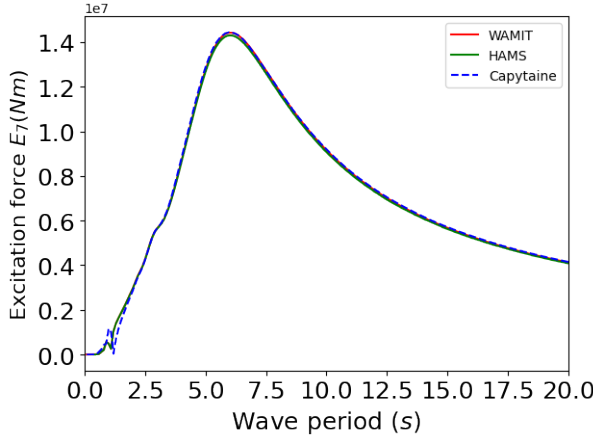Figure 4: Radiation damping flap B_{77}
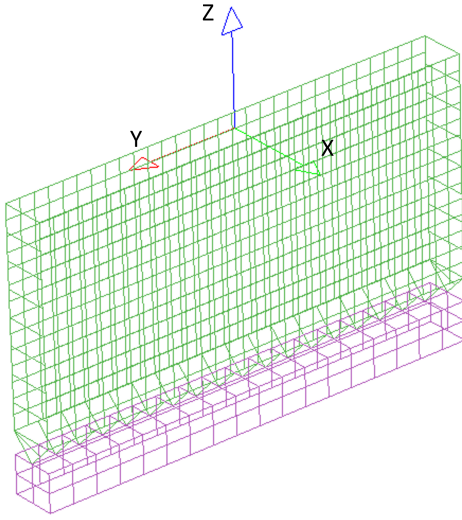
Figure 5: Excitation force flap E_7

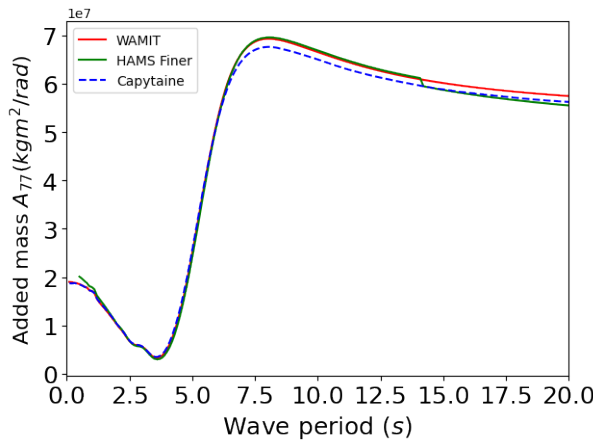Figure 6: Finer mesh of the flap in HAMS with 1012 panels - Top (green) and bottom (pink)

Figure 7: Added mass flap A_{77} with finer HAMS mesh for the flap top

however diffraction was considered. When modelling in Capytaine, a similar two-body simulation is performed, wherein the same shape functions as derived earlier are utilized for the top and bottom of the flap. This utilizes the 'Customized degree of freedom' option in Capytaine. Lower order panels were utilized for all simulations to solve both diffraction and radiation problems.

The results of the hydrodynamic coefficients (added mass coefficient and radiation damping coefficient) for the additional degree of freedom are shown in Figure 3 and Figure 4 respectively. When comparing the added mass (noted as A_{77}) for the three solvers, it can be observed that Capytaine is closer to WAMIT up to the wave period of 4 s. Between 4 and 6 s, both HAMS and Capytaine are very close to WAMIT. Between 6 and 14 s, HAMS is very close to WAMIT. However for wave periods 6 s onwards, Capytaine is found to slightly underestimate the response (approximately 3%) in comparison to WAMIT for the rest of the wave periods investigated. With HAMS, at 14 s, there is a sudden change leading to a consistent underestimation (about 5-6%) as compared to WAMIT. Capytaine is closer to WAMIT in these range of periods. The peaks for all three solvers are observed to occur at the same wave period. The peak of HAMS and WAMIT is very close, while Capytaine slightly underestimates the peak.

When considering the radiation damping coefficient (noted as B_{77}), all the solvers are generally quite close with Capytaine being closer to WAMIT till wave period of 6 s, while HAMS is much closer to WAMIT from 6 to 12.5 s wave periods; however, HAMS shows a slightly higher values at around the wave period of 5 s. Considering the peaks of the radiation damping coefficient, Capytaine is closer to WAMIT than HAMS.

The results for the excitation forces E_7 are shown in Figure 5. When considering the excitation forces, all solvers are found to produce similar values. The peaks are also very close.

An unusual drop is observed at the low period of 1 s in both the radiation damping coefficient and excitation force, and is less pronounced in the added mass coefficient. This can be attributed to the irregular frequency, which is usually observed at high wave frequencies. This can be nullified by using a waterplane mesh in addition to the hull mesh, and solving the extended boundary value problem (Liu 2019). This is however, not investigated in this research.

In order to further improve the results of the added mass, an additional simulation was performed increasing the mesh resolution of the flap top (see Figure 6). The results for the added mass A_{77} with the finer mesh are shown in Figure 7. As observed, HAMS is now closer to WAMIT between 0 and 14 s wave periods, but beyond this limit, it agrees well with Capytaine.

Table 2: Comparison of Capytaine and HAMS

Solver	Parallelization	N_p	N_f	DOF	Time(s)
HAMS	No	518	270	7	780
Capytaine	No	518	270	1	890
HAMS	Yes	518	270	7	430
Capytaine	Yes	518	270	1	94
HAMS finer	Yes	1012	270	7	1040

5 COMPUTATIONAL RESOURCES

The device utilized for running the simulations in HAMS and Capytaine is a 64-bit laptop with 16GB RAM, 8 cores and Intel i7-1185G7 of 3.00 GHz CPU.

The comparison of the computational effort between HAMS and Capytaine is shown in Table 2. 270 periods between 0.1 s and 27.1 s were considered for the analysis. Since no reference to computational time was provided for WAMIT in the work of Van 'T Hoff (Van 'T Hoff 2009), this was not included. With the current implementation in HAMS, the only option available is to run all degrees of freedom together. This entails the six rigid body modes and any additional modes (in this case the pitching of the flap about the hinge). In Capytaine, it is possible to run the simulations considering specific degrees of freedom. Therefore, simulations were run just for the additional degree of freedom. N_p refers to the number of panels utilized in each model, N_f is the number of periods considered and DOF is the degrees of freedom considered in the simulation.

HAMS uses OpenMP parallelization while Capytaine allows for two types of parallelization –through $OpenMP$ and through $joblib$. When solving a single problem, matrix constructions and linear algebra operations can be parallelized through $OpenMP$. This can be controlled using the environment variable `OMP_NUM_THREADS` on a Windows system. When solving multiple problems, $joblib$ can be utilized in addition to $OpenMP$ to run multiple jobs. The calculations performed with 8 threads in Capytaine as seen in Table 2 were performed utilizing both $OpenMP$ and $joblib$ with running 8 jobs simultaneously.

From Table 2, it can be observed that HAMS is slightly faster without parallelization than Capytaine even considering 7 degrees of freedom as compared to 1 degree of freedom in Capytaine. With parallelization, Capytaine is 5 times faster than HAMS, but this considering 7 degrees of freedom in HAMS as compared to 1 degree of freedom in Capytaine. The simulation time for HAMS with the finer mesh is also shown in Table 2.

6 LIMITATIONS

With the introduction of the generalized modes approach in HAMS, it is possible to analyse structures with constraints. With this implementation, a general shape function describing the body surface boundary condition can be given as input for the additional mode to solve the diffraction and radiation problem,

in addition to the 6 rigid body modes. The current research showcases this implementation considering the flap converter as an example. The adopted methodology for deriving the shape function can be utilized to fixed and floating structures with single hinges. If there are more hinges, this methodology can be extended to structures with multiple hinges by assuming unit rotation about each hinge and obtaining the corresponding shape function.

7 CONCLUDING REMARKS

This work showcases the extension of the open-source BEM solver HAMS to incorporate the generalized modes. This is done by deriving a shape function, that describes the additional degree of freedom/mode shape, and modifying the body boundary condition within the BEM solver to incorporate it. To demonstrate this methodology in HAMS, the case of a hinged rigid flap is considered. A two body diffraction and radiation problem is solved considering the pitch motion about the hinge for the flap top and no degrees of freedom for the flap bottom.

Cross-model validation with commercial solver WAMIT is performed for the hydrodynamic coefficients and excitation forces using the work of Van 'T Hoff Van 'T Hoff (2009). Furthermore, a comparison is also made with open-source BEM solver Capytaine, comparing the hydrodynamic coefficients and excitation forces, as well as the computational effort. When comparing the added mass coefficient, it is observed that HAMS is generally close to WAMIT with slight overestimation till wave periods of 5 s and slight underestimation of the added mass coefficient for wave periods of 14 s or higher. In these ranges of wave periods, Capytaine is closer to WAMIT. Considering the radiation damping coefficient and excitation forces, all solvers are close. In order to improve the estimation of the added mass coefficient in HAMS, an additional simulation was run with a higher resolution mesh, which improved the results for both 0-5 s and above 14 s wave periods, however still slightly underestimating the added mass coefficient beyond wave period of 14 s.

When comparing the computational effort between HAMS and Capytaine for the diffraction/radiation problem, it can be observed that HAMS is slightly faster without parallelization than Capytaine even considering 7 degrees of freedom as compared to 1 degree of freedom in Capytaine. With parallelization, Capytaine is 5 times faster than HAMS, but this is considering 7 degrees of freedom in HAMS as compared to 1 degree of freedom in Capytaine. In HAMS, with the current implementation, the calculation is performed for all considered degrees of freedom (rigid modes + additional modes). However, in Capytaine, it is possible to just run the diffraction/radiation calculations for a specific degree of freedom. Hence, the comparison here is done with 7

degrees of freedom in HAMS, as compared to 1 in Capytaine.

With the implementation of generalized modes in open-source solver HAMS, it can now be utilized for the hydrodynamic modelling of flexible structures or structures with constraints thus adding to the open-source domain and accelerating energy transition.

8 ACKNOWLEDGEMENTS

REFERENCES

Ancellin, M. & F. Dias (2019, 04). Capytaine: a python-based linear potential flow solver. *Journal of Open Source Software 4*, 1341.

Ancellin, M., M. Dong, P. Jean, & F. Dias (2020). Far-field maximal power absorption of a bulging cylindrical wave energy converter. *Energies 13*(20).

ANSYS (2012). *ANSYS AQWA v14.5*. ANSYS, Inc.

Babarit, A. & G. Delhommeau (2015, September). Theoretical and numerical aspects of the open source BEM solver NEMOH. In *11th European Wave and Tidal Energy Conference (EWTEC2015)*, Proceedings of the 11th European Wave and Tidal Energy Conference, Nantes, France.

Babarit, A., F. Wendt, Y.-H. Yu, & J. Weber (2017). Investigation on the energy absorption performance of a fixed-bottom pressure-differential wave energy converter. *Applied Ocean Research 65*, 90–101.

EC (2020). EU Strategy for Offshore Renewables. Accessed: 2023-07-10.

Falcão, A. (2010). Wave energy utilization: A review of the technologies. *Renewable and Sustainable Energy Reviews 14*(3), 899–918.

Gomes, R., M. Lopes, J. Henriques, L. Gato, & A. Falcão (2015). The dynamics and power extraction of bottom-hinged plate wave energy converters in regular and irregular waves. *Ocean Engineering 96*, 86–99.

Lee, C.-H. & J. N. Newman (2003). Computation of wave effects using the panel method.

Lee, C. H. & J. N. Newman (2006). *WAMIT User Manual, Versions 7, 6.4, 6.4PC, 6.3S, 6.3S-PC*. WAMIT, Inc.

Liu, Y. (2019). HAMS: A frequency-domain preprocessor for wave-structure interactions—theory, development, and application. *Journal of Marine Science and Engineering 7*(3).

Liu, Y., S. Yoshida, C. Hu, M. Sueyoshi, L. Sun, J. Gao, P. Cong, & G. He (2018). A reliable open-source package for performance evaluation of floating renewable energy systems in coastal and offshore regions. *Energy Conversion and Management 174*, 516–536.

Newman, J. (1994). Wave effects on deformable bodies. *Applied Ocean Research 16*(1), 47–59.

Raghavan, V., G. Lavidas, A. Metrikine, N. Mantadakis, & E. Loukogeorgaki (2022, 10). A comparative study on BEM solvers for wave energy converters. pp. 441–447. CRC Press.

Sheng, W., E. Tapoglou, X. Ma, C. Taylor, R. Dorrell, D. Parsons, & G. Aggidis (2022). Hydrodynamic studies of floating structures: Comparison of wave-structure interaction modelling. *Ocean Engineering 249*, 110878.

Sismani, G. & E. Loukogeorgaki (2020). Frequency-based investigation of a floating wave energy converter system with multiple flaps. *Applied Mathematical Modelling 84*, 522–535.

van Rij, J., Y.-H. Yu, & Y. Guo (2017, 06). Structural loads analysis for wave energy converters. pp. V010T09A023.

Van 'T Hoff, J. (2009). *Hydrodynamic modelling of the oscillating wave surge converter*. Ph. D. thesis, Queens University Belfast.